Available online at www.sciencedirect.com
SCIENCE DIRECT®
Journal of Computational Physics 196 (2004) 282–297
JOURNAL OF COMPUTATIONAL PHYSICS
www.elsevier.com/locate/jcp

3-D wave simulation in anelastic media using the Kelvin–Voigt constitutive equation

José M. Carcione, Flavio Poletto, Davide Gei *

Istituto Nazionale di Oceanografia e di Geofisica Sperimentale (OGS), Borgo Grotta Gigante 42c, 34010 Sgonico, Trieste, Italy

Received 14 July 2003; received in revised form 28 October 2003; accepted 28 October 2003

Abstract

We design a numerical algorithm for wave simulation in anelastic media in the presence of free surface, which can be used to model seismic waves at the Earth's surface and ultrasonic waves in heterogeneous materials. The stress–strain relation is based on the Kelvin–Voigt mechanical model, which has the advantage of not requiring additional field variables. The model requires two anelastic parameters and twice the spatial derivatives of the lossless case. The high-frequency components of the wave field are more attenuated than the low-frequency components, with the attenuation factors being approximately proportional to the square of the frequency. The modeling simulates 3-D waves by using the Fourier and Chebyshev methods to compute the spatial derivatives along the horizontal and vertical directions, respectively. We stretch the mesh in the vertical direction to increase the minimum grid spacing and reduce the computational cost. Instabilities of the Chebyshev differential operator due to the implementation of the free-surface boundary conditions are solved with a characteristic approach, where the characteristic variables are evaluated at the source central frequency. The results of the modeling are verified by comparisons to the analytical solutions for Lamb's problem and propagation in unbounded homogeneous media. Examples illustrating the propagation of Rayleigh and Love waves are presented.

Keywords: Simulation; Three-dimensional; Waves; Attenuation; Kelvin–Voigt model; Free surface; Seismic; Ultrasonic

1. Introduction

Wave modeling is a valuable tool for seismic interpretation and an essential part of inversion algorithms. Problems regarding environmental geophysics, seismic exploration, foundation engineering, earthquake seismology and non-destructive testing (NDT) of materials require the use of full-wave three-dimensional modeling methods [2,18,27,36]. In particular, it is important to model the surface waves (Rayleigh and Love waves) and record the three components of the wave field. Moreover, the unconsolidated nature of the shallow layers in many cases requires an anelastic stress–strain relation to model the dissipation of the wave field. An efficient and highly accurate technique is full-wave modeling by using pseudospectral methods [6,7,12,20].

* Corresponding author. Tel.: +39-040-2140321; fax: +39-040-327521.
E-mail address: dgei@ogs.trieste.it (D. Gei).

0021-9991/$ - see front matter © 2003 Elsevier Inc. All rights reserved.
doi:10.1016/j.jcp.2003.10.024

The calculation of three-dimensional synthetic seismograms by using pseudospectral differential operators has been introduced by Reshef et al. [35], who consider a lossless medium and model the free surface by the so-called "zero-padding" method. This approach requires to include a wide zone with zero P- and S-wave velocities above the upper surface of the model. The spatial derivatives along the three spatial dimensions are computed with the Fourier method. Generalizations of this algorithm to the elastic-anisotropic, viscoelastic-isotropic and viscoelastic-anisotropic cases are, respectively, given in Carcione et al. [14], Carcione [9] and Carcione [11]. However, the performance of the zero-padding method to model surface waves is not optimal, mainly when source and receiver are near the surface [34]. To overcome this problem, Kosloff et al. [24] and Tessmer and Kosloff [37] use the Chebyshev method to compute the derivatives along the vertical direction (they solve the elastic-isotropic wave equation). Unlike the Fourier method, the Chebyshev method is not periodic and allows for the incorporation of boundary conditions by using characteristic variables, in particular, free-surface conditions at the surface and non-reflecting conditions at the bottom of the mesh.

All the modeling algorithms mentioned above solve the wave equation in the space–time domain, where the incorporation of anelasticity requires the use of additional variables, called "memory variables" [12]. Generally, this approach is based on the use of the generalized Zener model [12] or the generalized Maxwell model [17]. Use of memory variables can be expensive in three dimensions, since the Zener model requires six variables for each relaxation mechanism [12]. A model which does not requires memory variables is the Kelvin–Voigt mechanical model [5,12]. We use this model to describe attenuation, because its implementation is simple and only requires the calculations of additional spatial derivatives and the use of two anelastic parameters compared to four parameters when using the Zener model. For instance, consider that the model is discretized in a cubic mesh with 81 grid points along each spatial direction. The number of unknown field variables using the velocity–stress formulation is nine (three particle-velocity components and six stress components). The Zener model requires six additional arrays to describe attenuation, and six arrays for the material properties (two Lamé constants and four relaxation times). Then, the total RAM storage occupied by the Zener model is 21×81^3, i.e., more than 11 Mwords. On the other hand, the Kelvin–Voigt model requires nine arrays for the field variables and four arrays for the material properties, implying a computer storage of less than 7 Mwords. Therefore, the saving in storage is more than 35%. The drawback is that the Kelvin–Voigt model requires the calculation of nine additional spatial derivatives at each time step, compared to the Zener model. However, the saving in computer storage can be significant when modeling general attenuation laws. In this case, the Zener model requires several elements, with the consequent increase in memory-variable storage. Note that the Zener model describes a single attenuation peak, while the Kelvin–Voigt dissipation factor is linear with frequency. Another feature compared to the Zener model is that the phase velocity of the waves tends to ∞ at the high-frequency limit, but this is not a major problem when using band-limited source functions. The Kelvin–Voigt law can be used to model scattering attenuation or loss due to interlayer flow at low frequencies [22]. General attenuation curves can be described by using several elements [5,32].

The wave equation combines the equation of momentum conservation with the constitutive relations for isotropic and anelastic media based on the Kelvin–Voigt model. The velocity–stress formulation allows the calculation of the particle velocity and stress components simultaneously.

2. Equation of motion

The three-dimensional equations of momentum conservation can be expressed as

$$\rho \ddot{u}_i = \frac{\partial \sigma_{ij}}{\partial x_j} + f_i, \tag{1}$$

where ρ is the density, u_i are the displacement components, σ_{ij} denote the stress components, and f_j are the body forces. A dot above a variable denotes time differentiation and the Einstein convention for repeated indices is used.

The stress–strain relations for a Kelvin–Voigt solid are a simple generalization of those for one-dimensional media [12]. They are

$$\sigma_{ij} = (\lambda\theta + \lambda'\dot{\theta})\delta_{ij} + 2\mu\epsilon_{ij} + 2\mu'\dot{\epsilon}_{ij}, \tag{2}$$

where λ and μ are the Lamé constants, λ' and μ' are the corresponding anelastic parameters,

$$\epsilon_{ij} = \frac{1}{2}\left(\frac{\partial u_i}{\partial x_j} + \frac{\partial u_j}{\partial x_i}\right) \tag{3}$$

are the strain components,

$$\theta = \frac{\partial u_i}{\partial x_i} \tag{4}$$

and δ_{ij} is Kronecker's delta.

3. Frequency-domain analysis

In the frequency domain, Eq. (2) can be written as

$$\sigma_{ij} = \Lambda\theta\delta_{ij} + 2\Sigma\epsilon_{ij}, \tag{5}$$

where

$$\Lambda = \lambda + \mathrm{i}\omega\lambda' \quad \text{and} \quad \Sigma = \mu + \mathrm{i}\omega\mu' \tag{6}$$

are the complex Lamé moduli and ω is the angular frequency. Use of the correspondence principle [12] allows the calculation of the phase velocity and quality factor versus frequency. They are given by [12]

$$v_{\mathrm{p}} = \left[\mathrm{Re}\left(\frac{1}{v}\right)\right]^{-1} \tag{7}$$

and

$$Q = \frac{\mathrm{Re}\,(v^2)}{\mathrm{Im}\,(v^2)}, \tag{8}$$

where v is either the P-wave complex velocity or the S-wave complex velocity, given by

$$v(\mathrm{P}) = \sqrt{\frac{\Lambda + 2\Sigma}{\rho}} \quad \text{and} \quad v(\mathrm{S}) = \sqrt{\frac{\Sigma}{\rho}}, \tag{9}$$

respectively, and Re and Im take real and imaginary parts. The phase velocities of the P and S waves tend to $\sqrt{E/\rho}$ and $\sqrt{\mu/\rho}$ for $\omega \to 0$, and to ∞ for $\omega \to \infty$, where $E = \lambda + 2\mu$. The P- and S-wave quality factors are simply

$$Q_{\mathrm{P}} = \frac{E}{\omega E'} \quad \text{and} \quad Q_{\mathrm{S}} = \frac{\mu}{\omega\mu'}, \tag{10}$$

where $E' = \lambda' + 2\mu'$. The attenuation factor is given by [12]

$$\alpha = \frac{\omega}{v_p}[\sqrt{1+Q^2} - Q], \tag{11}$$

where v_p and Q are the phase velocity and quality factor of the P wave or S wave. For low-loss media ($Q \gg 1$), Eq. (11) becomes

$$\alpha(\mathrm{P}) = \frac{\omega^2 E'}{2E v_p} \quad \text{and} \quad \alpha(\mathrm{S}) = \frac{\omega^2 \mu'}{2\mu v_p}, \tag{12}$$

where Eqs. (10) have been used. Then, the attenuation factor is approximately proportional to the square of the frequency if the variation of the phase velocity is small over the range of frequencies of the signal (see Section 6).

The anelastic parameters can be obtained from the quality factors at a given frequency, say, the central frequency of the source, ω_0. We obtain

$$\lambda' = \frac{1}{\omega_0}\left(\frac{E}{Q_{\mathrm{P0}}} - \frac{2\mu}{Q_{\mathrm{S0}}}\right) \quad \text{and} \quad \mu' = \frac{\mu}{\omega_0 Q_{\mathrm{S0}}}, \tag{13}$$

where Q_{P0} and Q_{S0} are the quality factors at $\omega = \omega_0$, and E and μ are the moduli at $\omega = 0$.

The moduli can be obtained from the P- and S-wave phase velocities at $\omega = \omega_0$, $v_{\mathrm{p0}}(\mathrm{P})$ and $v_{\mathrm{p0}}(\mathrm{S})$, respectively. Using Eqs. (6), (7), (9) and (10) gives

$$E = \rho v_{\mathrm{p0}}^2(\mathrm{P}) g(Q_{\mathrm{P0}}) \quad \text{and} \quad \mu = \rho v_{\mathrm{p0}}^2(\mathrm{S}) g(Q_{\mathrm{S0}}), \tag{14}$$

where

$$g(a) = \frac{1}{2}(1+a^{-2})^{-1/2}[1 + (1+a^{-2})^{-1/2}]. \tag{15}$$

Note that $g(a) \to 1$ when $a \to \infty$. Hence, the input properties to the modeling program are ρ, $v_{\mathrm{p0}}(\mathrm{P})$, $v_{\mathrm{p0}}(\mathrm{S})$, Q_{P0} and Q_{S0}.

4. Velocity–stress formulation

Introducing the particle-velocity components, $v_i = \dot{u}_i$, the equations of momentum conservation (1) become

$$\dot{v}_i = \frac{1}{\rho}\left(\frac{\partial \sigma_{ij}}{\partial x_j} + f_i\right). \tag{16}$$

Using Eqs. (3) and (4), the time derivative of the stress–strain relations (2) become

$$\dot{\sigma}_{ij} = \left(\lambda \frac{\partial v_i}{\partial x_i} + \lambda' \frac{\partial \dot{v}_i}{\partial x_i}\right)\delta_{ij} + \mu\left(\frac{\partial v_i}{\partial x_j} + \frac{\partial v_j}{\partial x_i}\right) + \mu'\left(\frac{\partial \dot{v}_i}{\partial x_j} + \frac{\partial \dot{v}_j}{\partial x_i}\right). \tag{17}$$

Substituting (16) into (17) yields

$$\dot{\sigma}_{ij} = \lambda \frac{\partial v_i}{\partial x_i}\delta_{ij} + \lambda'\left[\frac{\partial}{\partial x_i}\frac{1}{\rho}\left(\frac{\partial \sigma_{ij}}{\partial x_j} + f_i\right)\right]\delta_{ij} + \mu\left(\frac{\partial v_i}{\partial x_j} + \frac{\partial v_j}{\partial x_i}\right) + \mu'\left[\frac{\partial}{\partial x_j}\frac{1}{\rho}\left(\frac{\partial \sigma_{im}}{\partial x_m} + f_i\right) + \frac{\partial}{\partial x_i}\frac{1}{\rho}\left(\frac{\partial \sigma_{jm}}{\partial x_m} + f_j\right)\right]. \tag{18}$$

Let us express the velocity–stress formulation in explicit form. Define the quantities

$$\begin{aligned} \Pi_x &= \frac{1}{\rho}\left(\frac{\partial \sigma_{xx}}{\partial x} + \frac{\partial \sigma_{xy}}{\partial y} + \frac{\partial \sigma_{xz}}{\partial z} + f_x\right), \\ \Pi_y &= \frac{1}{\rho}\left(\frac{\partial \sigma_{xy}}{\partial x} + \frac{\partial \sigma_{yy}}{\partial y} + \frac{\partial \sigma_{yz}}{\partial z} + f_y\right), \\ \Pi_z &= \frac{1}{\rho}\left(\frac{\partial \sigma_{xz}}{\partial x} + \frac{\partial \sigma_{yz}}{\partial y} + \frac{\partial \sigma_{zz}}{\partial z} + f_z\right), \end{aligned} \tag{19}$$

$$\psi = \frac{\partial \Pi_x}{\partial x} + \frac{\partial \Pi_y}{\partial y} + \frac{\partial \Pi_z}{\partial z} \tag{20}$$

and

$$\vartheta = \dot{\theta} = \frac{\partial v_x}{\partial x} + \frac{\partial v_y}{\partial y} + \frac{\partial v_z}{\partial z}. \tag{21}$$

Then, Eqs. (16) and (18) can be written in components as

$$\begin{aligned} \dot{v}_x &= \Pi_x, \\ \dot{v}_y &= \Pi_y, \\ \dot{v}_z &= \Pi_z, \end{aligned}$$

$$\begin{aligned} \dot{\sigma}_{xx} &= \lambda\vartheta + \lambda'\psi + 2\mu\frac{\partial v_x}{\partial x} + 2\mu'\frac{\partial \Pi_x}{\partial x}, \\ \dot{\sigma}_{yy} &= \lambda\vartheta + \lambda'\psi + 2\mu\frac{\partial v_y}{\partial y} + 2\mu'\frac{\partial \Pi_y}{\partial y}, \\ \dot{\sigma}_{zz} &= \lambda\vartheta + \lambda'\psi + 2\mu\frac{\partial v_z}{\partial z} + 2\mu'\frac{\partial \Pi_z}{\partial z}, \end{aligned} \tag{22}$$

$$\begin{aligned} \dot{\sigma}_{xy} &= \mu\left(\frac{\partial v_x}{\partial y} + \frac{\partial v_y}{\partial x}\right) + \mu'\left(\frac{\partial \Pi_x}{\partial y} + \frac{\partial \Pi_y}{\partial x}\right), \\ \dot{\sigma}_{xz} &= \mu\left(\frac{\partial v_x}{\partial z} + \frac{\partial v_z}{\partial x}\right) + \mu'\left(\frac{\partial \Pi_x}{\partial z} + \frac{\partial \Pi_z}{\partial x}\right), \\ \dot{\sigma}_{yz} &= \mu\left(\frac{\partial v_y}{\partial z} + \frac{\partial v_z}{\partial y}\right) + \mu'\left(\frac{\partial \Pi_y}{\partial z} + \frac{\partial \Pi_z}{\partial y}\right). \end{aligned}$$

Eqs. (19) and (22) constitute the velocity–stress formulation for the Kelvin–Voigt model. The model requires three arrays for the particle-velocity components, six arrays for the stress-tensor components, and four arrays for the material properties. On the other hand, the equation of motion based on a single Zener model requires six additional arrays for the memory variables and two additional arrays for the material

properties. The extra cost to avoid these memory requirements is the calculation of the nine additional spatial derivatives corresponding to the acceleration components.

5. Algorithm

The numerical solution is obtained by using a fourth-order Runge–Kutta method as time-stepping algorithm, the Chebyshev differential operator to compute the spatial derivatives along the vertical direction, and the Fourier differential operator along the horizontal directions. The Fourier and Chebyshev methods [6,7,12,20] consist of a spatial discretization and calculation of spatial derivatives using the fast Fourier transform. The Fourier method is a collocation technique in which a continuous function is approximated by a truncated series of trigonometric functions, wherein the spectral (expansion) coefficients are chosen such that the approximate solution coincides with the exact solution at the discrete set of sampling or collocation points. The collocation points are defined by equidistant sampling points. Since the expansion functions are periodic, the Fourier method is appropriate for problems with periodic boundary conditions. In the Chebyshev method, the collocation points are the roots of the Chebyshev polynomials. It is appropriate for simulating Neumann and Dirichlet boundary conditions. The Fourier and Chebyshev methods are infinitely accurate up to the maximum wavenumber of the mesh, that corresponds to a spatial wavelength of two grid points (at maximum grid spacing for the Chebyshev operator).

The conventional Chebyshev method has two major disadvantages. In the first place, the grid points are restricted to the Gauss–Lobatto collocation points. This poses a limitation regarding the location of the interfaces. Secondly, the clustering of grid points at the ends of the mesh restricts the time step of the time integration scheme, which has to be of the order $O(N^{-2})$ where N is the number of grid points. Here, we use a mapping transformation for the vertical coordinate which circumvents the severe stability condition of the integration method and distribute grid points in arbitrary locations. By stretching the mesh, we increase the minimum grid spacing and are able to increase the time step of the Runge–Kutta algorithm, thus reducing the computer time. For this purpose we have implemented the stretching function and algorithm described by Kosloff and Tal-Ezer [26], who claim to obtain time steps of the order $O(N^{-1})$. This has been verified by Renaut and Fröhlich [33] for the 2-D acoustic wave equation. Furthermore, this transformation can be used for spatial grid adaptation [1,3,21], in the sense that the collocation points can be redistributed and properly concentrated in regions with steep velocity gradients, fine layering and complex interface geometries. Similar mapping transformations can be applied in the horizontal directions, where the Fourier differential operator is used [19]. In particular, the time step depends on the size of the first grid cell at the end of the mesh. In general, stability can be achieved with the condition satisfied by the Fourier method. For the Runge–Kutta method the condition is [23]: $v\,\mathrm{d}t/\mathrm{d}z < 2.79$, where v is the maximum wave velocity, $\mathrm{d}t$ is the time step and $\mathrm{d}z$ is the minimum grid spacing.

The parabolic nature of the Kelvin–Voigt wave equation implies a lower limit for the allowed quality factor. Below this limit, the propagation becomes essentially diffusive. This can be shown with a one-dimensional analysis. In 1-D space, the particle velocity–stress equations (22) simplify to

$$\dot{\mathbf{V}} \equiv \begin{pmatrix} \dot{v} \\ \dot{\sigma} \end{pmatrix} = \begin{pmatrix} 0 & \rho^{-1}\partial/\partial_x \\ \lambda\partial/\partial_x & (\lambda'/\rho)\partial^2/\partial_x^2 \end{pmatrix} \begin{pmatrix} v \\ \sigma \end{pmatrix} \equiv \mathbf{M}\mathbf{V}, \tag{23}$$

where v and σ denote particle velocity and stress, respectively. Substituting the kernel $\mathbf{V}_0 \exp(\mathrm{i}\kappa x - \mathrm{i}\omega t)$ into Eq. (23) gives the dispersion equation

$$\mathrm{i}\omega = \frac{2}{\kappa}\left(\frac{\lambda'\kappa}{\rho} \pm \sqrt{\frac{\lambda'^2\kappa^2}{\rho^2} - \frac{4\lambda}{\rho}}\right), \tag{24}$$

where ω is a complex quantity and κ is the real wavenumber. The field maintains its wave character when the argument of the square root is negative, such that the frequency ω has a real component. This condition implies $\lambda' < 2\sqrt{\lambda\rho}/\kappa$. Using Eq. (13), the condition on the quality factor is $Q_{\mathrm{P0}} > \kappa\sqrt{\lambda/\omega_0}/\omega_0 \approx \kappa v_{\mathrm{p0}}(\mathrm{P})/\omega_0$. At the Nyquist wavenumber $\kappa = \pi/\mathrm{d}x$, where $\mathrm{d}x$ is the grid spacing, this condition gives

$$Q_{\mathrm{P0}} > \frac{v_{\mathrm{p0}}}{2f_0\,\mathrm{d}x}, \tag{25}$$

where $f_0 = \omega_0/(2\pi)$. If $v_{\mathrm{p0}} = 2000$ m/s, $f_0 = 50$ Hz and $\mathrm{d}x = 5$ m, we obtain $Q_{\mathrm{P0}} = 4$.

Numerical dispersion is due to the time discretization, since the spatial differential operators have spectral accuracy. The determination of the time step $\mathrm{d}t$ to obtain accurate solutions is particularly important in anelastic media, where physical dispersion should not be affected by numerical dispersion. It can be shown that the fourth-order Runge–Kutta discretization of Eq. (23) implies [23]

$$\mathbf{V}^{n+1} = \sum_{m=0}^{4} \frac{1}{m!}(\mathbf{M}\,\mathrm{d}t)^m \mathbf{V}^n, \tag{26}$$

where $t = n\,\mathrm{d}t$. Consider now that the frequency is real and the wavenumber k is complex. Substituting the kernel $\exp(\mathrm{i}kx - \mathrm{i}\omega n\,\mathrm{d}t)$ into Eq. (26) and taking the determinant of the system equal to zero gives

$$\det\left[(1 - \exp(\mathrm{i}\omega\,\mathrm{d}t))\mathbf{I} + \sum_{m=1}^{4} \frac{1}{m!}(\mathbf{M}\,\mathrm{d}t)^m\right] = 0, \tag{27}$$

where $\mathbf{I}$ is the 2×2 identity matrix, and $\mathbf{M}$ is a function of k. Solving for k, we define a complex velocity resulting from the Runge–Kutta approximation as

$$\bar{v} = \frac{\omega}{k}. \tag{28}$$

The phase velocity is then given by

$$\bar{v}_{\mathrm{p}} = \left[\mathrm{Re}\left(\frac{1}{\bar{v}}\right)\right]^{-1} \tag{29}$$

and the quality factor is

$$\bar{Q} = \frac{\mathrm{Re}\,(\bar{v}^2)}{\mathrm{Im}\,(\bar{v}^2)}. \tag{30}$$

The phase velocity and the quality factor depend on the time step $\mathrm{d}t$ which is determined to satisfy the accuracy requirements by comparing Eqs. (29) and (30) to the exact phase velocity (7) and quality factor (8). This approach has been used by Carcione and Quiroga-Goode [15] and Carcione et al. [13] to achieve accuracy for frequency-dependent stress–strain relations which model wave propagation in realistic media.

Boundary conditions are implemented by using a boundary treatment based on characteristics variables [10,24]. This method has been proposed by Bayliss et al. [4] to model free surface and non-reflecting boundary conditions. The wave equation is decomposed into outgoing and incoming wave modes perpendicular to the free surface. The outgoing waves are determined by the solution inside the domain, while the incoming waves are calculated from the boundary conditions. Let the vertical direction be parallel to

the z-axis. At each time step, the wave field at the boundaries is updated according to the following equations. At the upper boundary, the free-surface boundary equations are

$$v_x^{(\mathrm{new})} = v_x^{(\mathrm{old})} - \sigma_{xx}^{(\mathrm{old})}/Z_{\mathrm{S}}, \tag{31}$$

$$v_y^{(\mathrm{new})} = v_y^{(\mathrm{old})} - \sigma_{yy}^{(\mathrm{old})}/Z_{\mathrm{S}}, \tag{32}$$

$$v_z^{(\mathrm{new})} = v_z^{(\mathrm{old})} - \sigma_{zz}^{(\mathrm{old})}/Z_{\mathrm{P}}, \tag{33}$$

$$\sigma_{xx}^{(\mathrm{new})} = \sigma_{xx}^{(\mathrm{old})} - \frac{\lambda_0}{E_0}\sigma_{zz}^{(\mathrm{old})}, \tag{34}$$

$$\sigma_{yy}^{(\mathrm{new})} = \sigma_{yy}^{(\mathrm{old})} - \frac{\lambda_0}{E_0}\sigma_{zz}^{(\mathrm{old})}, \tag{35}$$

$$\sigma_{zz}^{(\mathrm{new})} = 0, \tag{36}$$

$$\sigma_{xz}^{(\mathrm{new})} = 0, \tag{37}$$

$$\sigma_{yz}^{(\mathrm{new})} = 0, \tag{38}$$

where $Z_{\mathrm{P}} = \rho v_{\mathrm{p0}}(\mathrm{P})$, $Z_{\mathrm{S}} = \rho v_{\mathrm{p0}}(\mathrm{S})$, $\lambda_0 = \rho(v_{\mathrm{p0}}^2(\mathrm{P}) - 2v_{\mathrm{p0}}^2(\mathrm{S}))$ and $E_0 = \rho v_{\mathrm{p0}}^2(\mathrm{P})$. We have considered the characteristics at the central frequency of the source. That is, velocities and impedances are taken at $\omega = \omega_0$ (see Section 3).

At the bottom of the mesh, the non-reflecting boundary equations are

$$v_x^{(\mathrm{new})} = 0.5(v_x^{(\mathrm{old})} + \sigma_{xz}^{(\mathrm{old})}/Z_{\mathrm{S}}), \tag{39}$$

$$v_y^{(\mathrm{new})} = 0.5(v_y^{(\mathrm{old})} + \sigma_{yz}^{(\mathrm{old})}/Z_{\mathrm{S}}), \tag{40}$$

$$v_z^{(\mathrm{new})} = 0.5(v_z^{(\mathrm{old})} + \sigma_{zz}^{(\mathrm{old})}/Z_{\mathrm{P}}), \tag{41}$$

$$\sigma_{xx}^{(\mathrm{new})} = \sigma_{xx}^{(\mathrm{old})} + \frac{\lambda_0}{E_0}(\sigma_{zz}^{(\mathrm{new})} - \sigma_{zz}^{(\mathrm{old})}), \tag{42}$$

$$\sigma_{yy}^{(\mathrm{new})} = \sigma_{yy}^{(\mathrm{old})} + \frac{\lambda_0}{E_0}(\sigma_{zz}^{(\mathrm{new})} - \sigma_{zz}^{(\mathrm{old})}), \tag{43}$$

$$\sigma_{zz}^{(\mathrm{new})} = 0.5(\sigma_{zz}^{(\mathrm{old})} + Z_{\mathrm{P}} v_z^{(\mathrm{old})}), \tag{44}$$

$$\sigma_{xz}^{(\mathrm{new})} = 0.5(\sigma_{xz}^{(\mathrm{old})} + Z_{\mathrm{S}} v_x^{(\mathrm{old})}), \tag{45}$$

$$\sigma_{yz}^{(\mathrm{new})} = 0.5(\sigma_{yz}^{(\mathrm{old})} + Z_{\mathrm{S}} v_y^{(\mathrm{old})}). \tag{46}$$

In addition to the non-reflecting conditions, absorbing strips are used to further attenuate the wave field at the bottom of the mesh [25]. This combined use of damping methods practically eliminates any wraparound caused by the Fourier operator at the boundaries of the mesh.

6. Simulations

In order to illustrate the physics of wave propagation, let us consider a dissipative medium with $\rho = 2.3$ g/cm^3, $v_{\mathrm{p0}}(\mathrm{P}) = 3.2$ km/s and $Q_{\mathrm{P0}} = 10$. These properties correspond to a reference frequency $f_0 = 50$ Hz. Fig. 1 shows the P-wave phase velocity and dissipation factor ($1/Q_{\mathrm{P}}$) versus frequency. The phase velocity and dissipation factor increase with frequency and tend to infinity for infinite frequency. Note that at 50 Hz the quality factor is equal to 10.

We first test the numerical solution against the analytical solution for Lamb's problem in lossless media. The analytical solution for a Poisson solid (Poisson ratio equal to 0.25), with source and receiver located at the surface has been obtained by Pekeris [29] (see Appendix A). We consider a P-wave velocity of 2000 m/s. The mesh has $81 \times 81 \times 81$ grid points, with a horizontal grid spacing $\mathrm{d}x = \mathrm{d}y = 5$ m and a vertical size of 380 m (including the absorbing strip at the bottom of the mesh). The source is a Ricker-type wavelet located at the surface and has a dominant frequency of 60 Hz. The receiver is located at the surface at 60 m from the source. The Runge–Kutta algorithm requires a time step of 0.5 ms. Fig. 2 shows the Green's function for Lamb's problem (a) and the comparison between the analytical solution (solid line) and numerical solution (dotted line) (b). The dashed line is the viscoelastic numerical solution for $Q_{\mathrm{P0}} = 30$ and $Q_{\mathrm{S0}} = 20$.

The second test compares the numerical solution with the analytical solution for wave propagation in lossy homogeneous media (see Appendix B). We consider the same medium of the previous test, a mesh with $81 \times 81 \times 81$ grid points, a horizontal grid spacing $\mathrm{d}x = \mathrm{d}y = 5$ m and a vertical size of 380 m. The source position is 174 m below the free surface and has a dominant frequency of 50 Hz. Fig. 3 shows the comparison for the vertical (a) and horizontal (b) particle velocities. The solid and dashed lines correspond to the viscoelastic and elastic analytical solutions, and the dotted line is the viscoelastic numerical solution. The two pulses are the P wave and the S wave. As can be seen, the agreement between numerical an analytical solutions is excellent.

The following example has been given in [8], where the Zener model has been used to describe the anelasticity and the modeling is two-dimensional. It represents a seismic experiment for environmental applications [38]. Fig. 4 shows the model properties, source location and the line of receivers. The media are

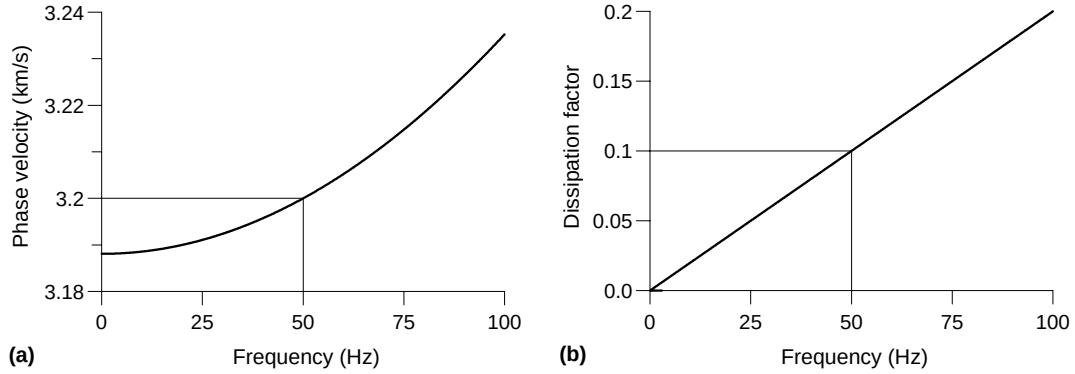

Fig. 1. P-wave phase velocity (a) and dissipation factor (Q_{P}^{-1}) (b) versus frequency. We have indicated the frequency at which the input properties are defined ($v_{\mathrm{p0}}(\mathrm{P}) = 3.2$ km and $Q_{\mathrm{P0}} = 10$ at $f_0 = 50$ Hz).

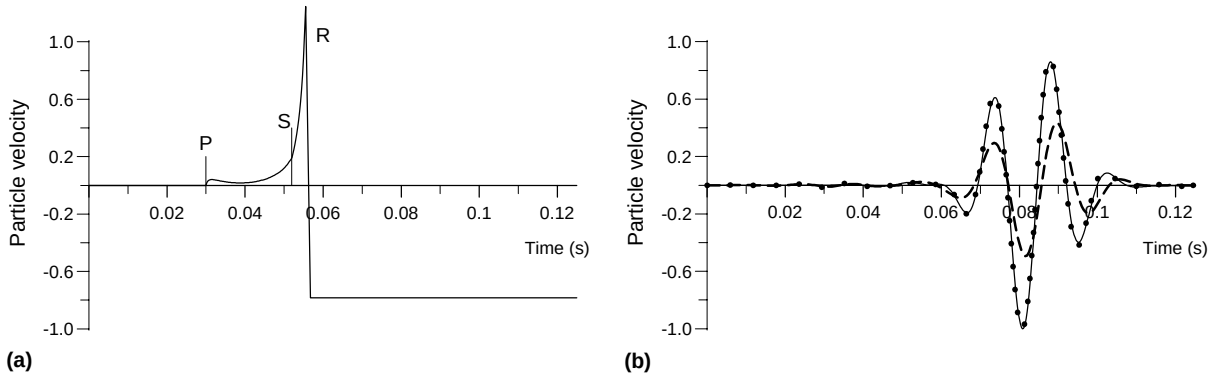

Fig. 2. Green's function for Lamb's problem (a) and comparison between the analytical solution (solid line) and numerical solution (dotted line) (b). The labels P, S and R indicate the P wave, the S wave and the Rayleigh wave. The dashed line is the viscoelastic numerical solution for $Q_{P0} = 30$ and $Q_{S0} = 20$. The source is a vertical force and the solution is the vertical particle velocity recorded at 60 m from the source (source and receiver are located at the surface). The dominant frequency is 60 Hz, the P-wave velocity is 2000 m/s and the medium is a Poisson solid. The P, S and Rayleigh wave arrival times are indicated.

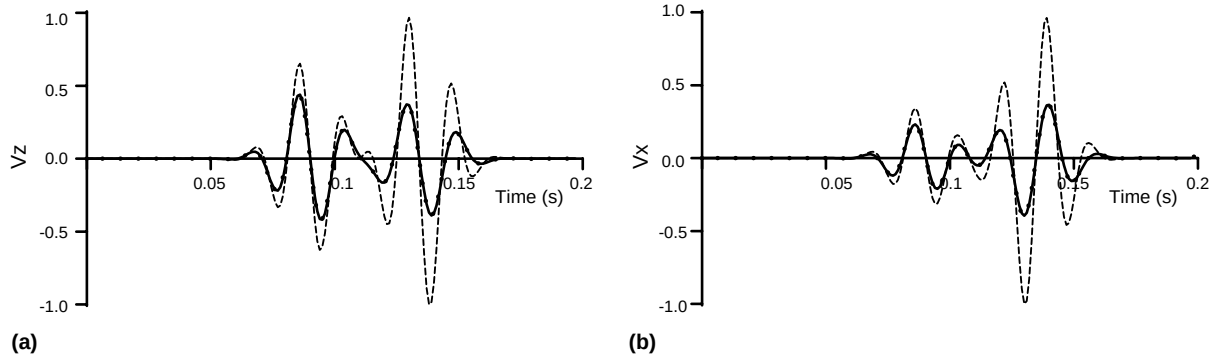

Fig. 3. Viscoelastic (solid line) and elastic (dashed line) analytical solutions, and numerical solution (dotted line) corresponding to the wave field generated by an impulsive force in a 3-D homogeneous medium. The vertical (a) and horizontal (b) particle velocities are shown. The source is a vertical force below the free surface, and the solution is the vertical particle velocity recorded at $(x_r, y_r, z_r) = (50, 50, 100)$ m with respect to the source position. The dominant frequency is 50 Hz and the medium is the same of the previous test (Fig. 2).

Poisson solids and the mesh are the same of the previous simulation. The source is a vertical force located at 2.5 m depth and has a dominant frequency of 50 Hz. Figs. 5 and 6 show the seismograms for the v_x and v_z components, where (a) corresponds to the lossless case and (b) to the lossy case. In this case we have assumed that the medium where the source is located (the incidence medium) has $Q_{P0} = 30$ and $Q_{S0} = 20$ (the reference frequency is equal to 50 Hz). The labels indicate the different waves, with "i", "r" and "t" denoting incident, reflected and transmitted, and "P" and "R" denoting compressional and Rayleigh, respectively. The incident Rayleigh wave (iR) arrives at the interface at 0.4 s and splits into a reflected Rayleigh wave (iRrR) and a transmitted Rayleigh wave (iRtR). In Figs. 5(b) and 6(b), we can see the attenuation of the Rayleigh wave (iR) in the incidence medium, while the transmitted Rayleigh wave (iRtR) only decays by geometrical spreading in the transmission medium. The reflected Rayleigh wave (iRrR) undergoes both, attenuation due to intrinsic dissipation and decay due to geometrical spreading.

Fig. 7 shows the model properties, source location and line of receivers for the simulation of Love waves. The properties of the media and the mesh are the same of the previous simulation. The source is a

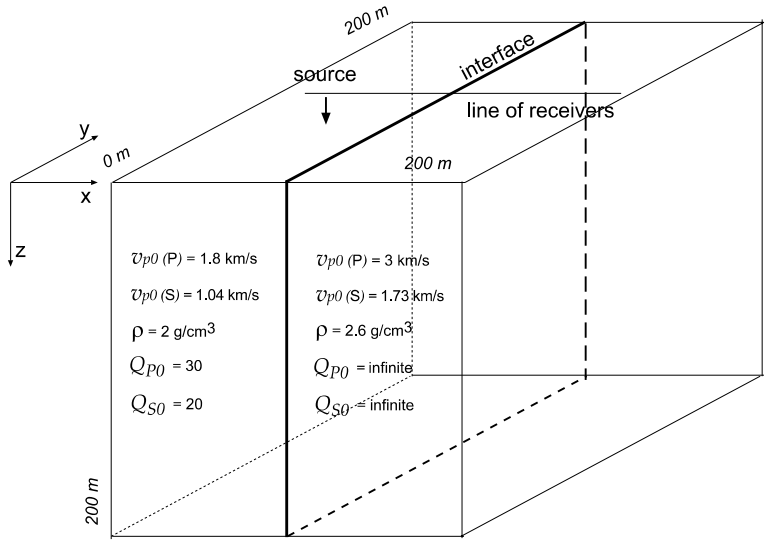

Fig. 4. Model, properties, and source and receiver locations to illustrate the propagation of Rayleigh waves. The media are Poisson solids.

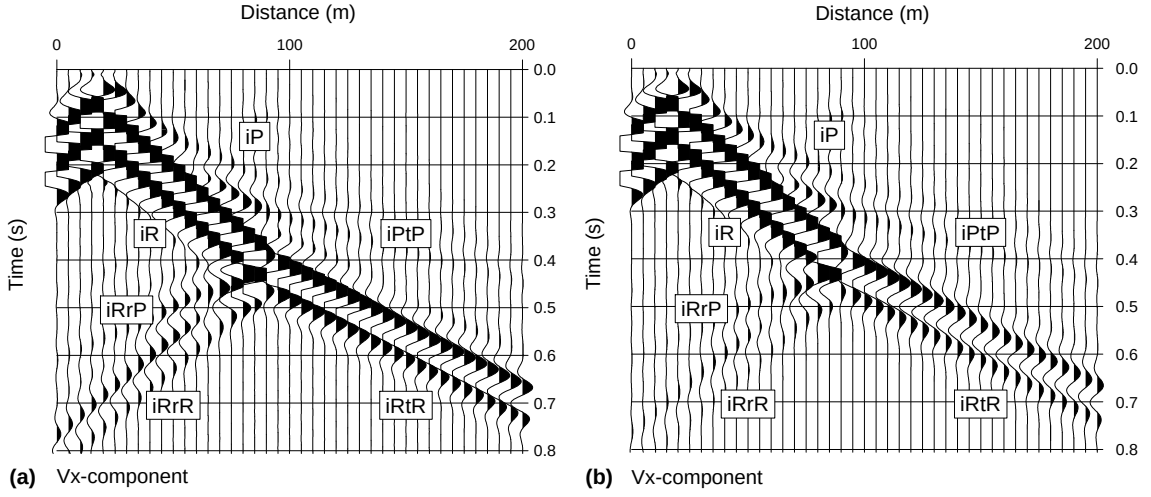

Fig. 5. Seismograms of the v_x component (see Fig. 4), where (a) corresponds to the lossless case and (b) to the lossy case. In this case, the incidence medium is viscoelastic. The labels indicate the different waves, with "i", "r" and "t" denoting incident, reflected and transmitted, and "P" and "R" denoting compressional and Rayleigh, respectively.

horizontal force located at 2.5 m depth and has a dominant frequency of 50 Hz. This source excites only Love surface waves in the receivers. A requirement is that the vertical section below the line of receivers be a plane of mirror symmetry. Fig. 8 compares v_y-component seismograms for the lossless (a) and lossy (b) cases. The dissipation of the train of dispersed Love waves can be observed.

Although the previous simulations use Poisson solids, the modeling is not restricted to this type of medium. As shown by Carcione [8] in the two-dimensional case, the algorithm can handle strong contrasts

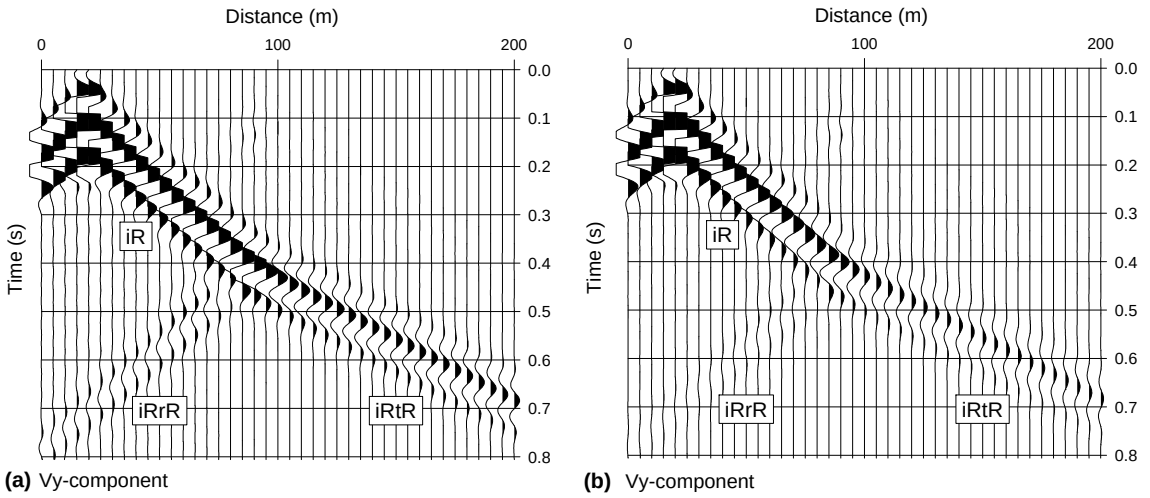

Fig. 6. Seismograms of the v_z component (see Fig. 4), where (a) corresponds to the lossless case and (b) to the lossy case. In this case, the incidence medium is viscoelastic. The labels indicate the different waves, with "i", "r" and "t" denoting incident, reflected and transmitted, and "P" and "R" denoting compressional and Rayleigh, respectively.

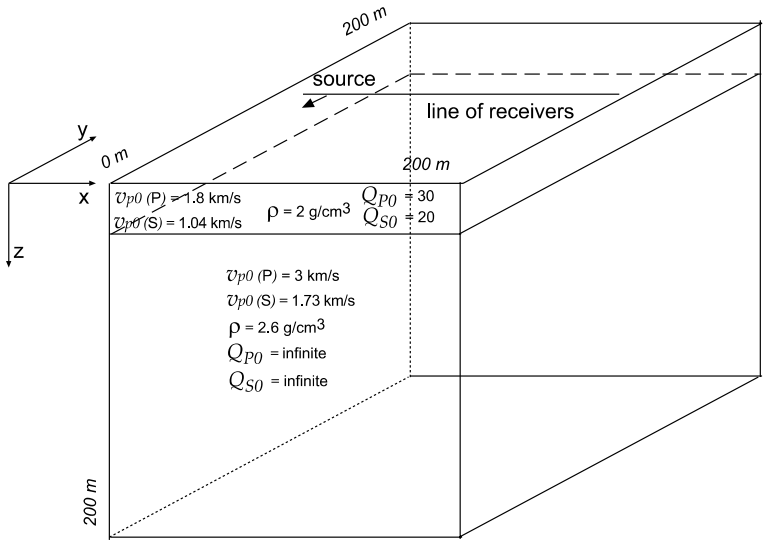

Fig. 7. Model, properties, and source and receiver locations to illustrate the propagation of Love waves. The media are Poisson solids.

in Poisson ratio (see also [31]). We have obtained stable results when computing the seismograms corresponding to Fig. 4 by replacing the low-velocity medium with a fluid, whose Poisson's ratio is 0.5 (we have considered $v_{p0}(S) = 0.1$ m/s). Moreover, note that the previous simulations may apply to any frequency range if we choose (scale) the source parameters, mesh attributes and reference frequency accordingly. Using the same mesh of the previous simulations, an example of ultrasonic propagation would require a grid spacing of 0.5 mm, a vertical size of 3.8 cm, a source central frequency of 500 kHz and a reference frequency of 500 kHz. Similarly, parameters for earthquake seismology can be a grid spacing of 1.3 km, a

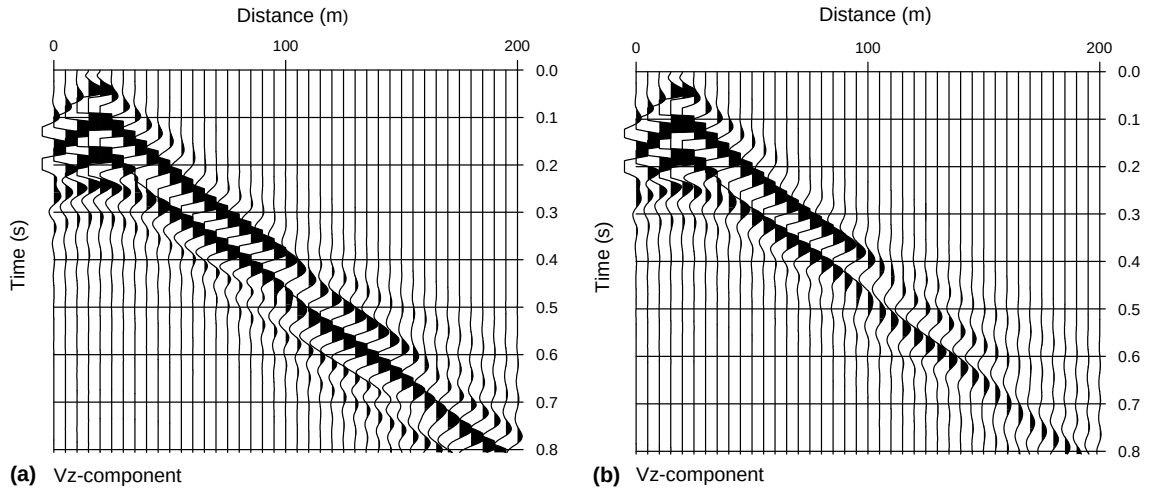

Fig. 8. Seismograms of the v_y component (see Fig. 7), where (a) corresponds to the lossless case and (b) to the lossy case. The surface layer is viscoelastic.

vertical size of 100 km, a source central frequency of 0.2 Hz and a reference frequency of 0.2 kHz. Unlike the differences in the distance and time scales, the seismograms corresponding to these applications will be similar to those shown in Figs. 5, 6 and 8 if the same density, velocity and quality-factor values are used.

7. Conclusions

We have developed a numerical approach for wave simulation in anelastic media in the presence of free surface. The modeling simulates 3-D waves by using the Fourier and Chebyshev methods to compute the spatial derivatives along the horizontal and vertical directions, respectively. The basic numerical algorithm has been used to model wave propagation in lossless media [37], for which the time step restriction is easier to determine. Here we adapt the algorithm to the lossy case (the boundary treatment mainly), and show how to determine the time step by analyzing the phase velocity and attenuation factor as a function of frequency. The stress–strain relation is based on the Kelvin–Voigt mechanical model. We have simulated Rayleigh and Love waves with intrinsic energy loss and showed that the difference with the lossless case are significant. The examples illustrate experiments for environmental applications, with realistic values of the quality factors and source dominant frequency in agreement with propagation in soils [38]. Moreover, the modeling is relevant to a number of applications, such as ultrasonic NDT testing, earthquake seismology and exploration seismic technology. The formulation based on one Kelvin–Voigt element models implies that the quality factor is linear as a function of frequency. In order to model a more general behaviour and match prescribed attenuation curves, a series connection of elements can be used [32]. The implementation of this general constitutive equation in 3-D wave modeling will be the subject of a future publication. Moreover, the modeling can easily be adapted to model topographic features and curved interfaces by using 3-D coordinate transformations [16].

Acknowledgements

Thanks to AGIP SpA (Exploration and Production Division) for funding in part the research. We are grateful to the associate editor and two anonymous referees for helpful comments.

Appendix A. Analytical solution for Lamb's problem

Pekeris [29] obtained a closed-form solution for the vertical surface displacement in response to a vertical point surface force of strength F_0, with a Heaviside function as time history. This solution has also been studied by Mooney [28]. Let us define the dimensionless time $\tau = (v_{p0}(S)/r)t$, where $r = \sqrt{x^2+z^2}$, $\delta = v_{p0}(P)/v_{p0}(S)$, and $\gamma = \sqrt{3+\sqrt{3}}$. The solution for a Poisson solid ($v_{p0}(P) = \sqrt{3}v_{p0}(S)$) is given by

$$G(\tau) = 0, \quad \tau < 1/\delta,$$
$$rG(\tau) = \begin{cases} -\frac{\pi}{96}\left\{6 - \sqrt{\frac{3\sqrt{3}+5}{\gamma^2-\tau^2}} + \sqrt{\frac{3\sqrt{3}-5}{\tau^2-\sqrt{3}/4-3/4}} - \sqrt{\frac{3}{\tau^2-1/4}}\right\}, & 1/\delta < \tau < 1, \\ -\frac{\pi}{48}\left\{6 - \sqrt{\frac{3\sqrt{3}+5}{\gamma^2-\tau^2}}\right\}, & 1 < \tau < \gamma, \\ -\pi/8, & \tau > \gamma. \end{cases} \tag{A.1}$$

The response to a Dirac's function (i.e., the Green's function) is the time derivative of (A.1). Another time differentiation is required to obtain the particle velocity. Then, the solution is given by $v_z = \ddot{G} * f = G * \ddot{f}$, where $f(t)$ is the time history of the source and $*$ denotes time convolution. f is a Ricker wavelet [12] and $\ddot{f}$ can be obtained analytically, while the convolution is performed by discretization of G and $\ddot{f}$ and using a numerical integration algorithm.

Appendix B. Analytical solution for unbounded homogeneous viscoelastic media

The solution of the displacement field generated by an impulsive point force in a 3-D elastic medium is given by Pilant [30]. Define the source–receiver distance as

$$r = \sqrt{x^2+y^2+z^2}, \tag{B.1}$$

and

$$\sin\theta = \frac{z}{r}, \quad \cos\theta = \frac{\sqrt{x^2+y^2}}{r}. \tag{B.2}$$

For a force acting in the positive z-direction, the radial and tangential components of the Green's function are

$$(4\pi\rho r\cos^{-1}\theta)G_r(r,\theta,\omega) = \left(\frac{1}{v_{p0}^2(P)} - \frac{2i}{v_{p0}(P)\omega r} - \frac{2}{\omega^2 r^2}\right)\exp[i\omega r/v_{p0}(P)] + \left(\frac{2i}{v_{p0}(S)\omega r} + \frac{2}{\omega^2 r^2}\right)\exp[i\omega r/v_{p0}(S)] \tag{B.3}$$

and

$$(4\pi\rho r\sin^{-1}\theta)G_\theta(r,\theta,\omega) = \left(-\frac{1}{v_{p0}^2(S)} + \frac{i}{v_{p0}(S)\omega r} + \frac{1}{\omega^2 r^2}\right)\exp[i\omega r/v_{p0}(S)] - \left(\frac{i}{v_{p0}(P)\omega r} + \frac{1}{\omega^2 r^2}\right)\exp[i\omega r/v_{p0}(P)], \tag{B.4}$$

respectively. The Cartesian horizontal and vertical components are then given by

$$G_x = G_y = \sin\theta G_r + \cos\theta G_\theta \tag{B.5}$$

and

$$G_z = \cos\theta G_r - \sin\theta G_\theta, \tag{B.6}$$

respectively. Using the correspondence principle [5,12], we replace the elastic wave velocities in (B.3) and (B.4) by the viscoelastic wave velocities $v(\mathrm{P})$ and $v(\mathrm{S})$ defined in Eq. (9). The 3-D viscoelastic Green's function components can then be expressed as

$$G_v(z,\omega) = G[z,\omega,v(\mathrm{P}),v(\mathrm{S})]. \tag{B.7}$$

Multiplication with the frequency-domain Fourier transform of the time derivative of the source time function and a numerical inversion by the discrete Fourier transform yield the desired time-domain solution.

References

[1] J.M. Augenbaum, An adaptive pseudospectral method for discontinuous problems, Appl. Numer. Math. 5 (1989) 459–480.
[2] E.A. Ash, E.G.S. Paige (Eds.), Rayleigh-wave Theory and Application, Springer, Berlin, 1985.
[3] A. Bayliss, Class, B.J. Matkowsky, Adaptive approximation of solutions to problems with multiple layers by Chebyshev pseudospectral methods, J. Comput. Phys. 116 (1995) 160–172.
[4] A. Bayliss, K.E. Jordan, B.J. LeMesurier, E. Turkel, A fourth-order accurate finite difference scheme for the computation of elastic waves, Bull. Seism. Soc. Am. 76 (1986) 1115–1132.
[5] A. Ben-Menahem, S.J. Singh, Seismic Waves and Sources, Springer, Berlin, 1981.
[6] J.P. Boyd, Chebyshev and Fourier Spectral Methods, Dover, New York, 2001.
[7] C. Canuto, M.Y. Hussaini, A. Quarteroni, T.A. Zang, Spectral Methods in Fluid Dynamics, Springer, Berlin, 1987, pp. 7–10.
[8] J.M. Carcione, Modeling anelastic singular surface waves in the Earth, Geophysics 57 (1992) 781–792.
[9] J.M. Carcione, Seismic modeling in viscoelastic media, Geophysics 58 (1993) 110–120.
[10] J.M. Carcione, Time-dependent boundary conditions for the 2-D linear anisotropic-viscoelastic wave equation, Numer. Meth. Part. Diff. Equations 10 (1994) 771–791.
[11] J.M. Carcione, Constitutive model and wave equation for linear, viscoelastic, anisotropic media, Geophysics 60 (1995) 537–548.
[12] J.M. Carcione, Wave Fields in Real Media. Theory and Numerical Simulation of Wave Propagation in Anisotropic, Anelastic and Porous Media, Pergamon Press, Oxford, 2001.
[13] J.M. Carcione, F. Cavallini, F. Mainardi, A. Hanyga, Time-domain seismic modeling of constant$Q$-wave propagation using fractional derivatives, Pure Appl. Geophys. 159 (2002) 1719–1736.
[14] J.M. Carcione, D. Kosloff, A. Behle, G. Seriani, A spectral scheme for wave propagation simulation in 3-D elastic-anisotropic media, Geophysics 57 (1992) 1593–1607.
[15] J.M. Carcione, G. Quiroga-Goode, Some aspects of the physics and numerical modeling of Biot compressional waves, J. Comput. Acous. 3 (1996) 261–280.
[16] J.M. Carcione, J.P. Wang, A Chebyshev collocation method for the elastodynamic equation in generalized coordinates, Comput. Fluid Dyn. J. 2 (1993) 269–290.
[17] H. Emmerich, M. Korn, Incorporation of attenuation into time-domain computations of seismic wave fields, Geophysics 52 (1987) 1252–1264.
[18] S.W. Fagin, Seismic modeling of geological structures: applications to exploration problems, in: Geophysical Development Series, vol. 2, Society of Exploration Geophysicists, 1992.
[19] B. Fornberg, The pseudospectral method: accurate representation of interfaces in elastic wave calculations, Geophysics 53 (1988) 625–637.
[20] B. Fornberg, A Practical Guide to Pseudospectral Methods, Cambridge University Press, Cambridge, 1996.
[21] H. Guillard, J.M. Malé, R. Peyret, Adaptive spectral methods with application to mixing layer computations, J. Comput. Phys. 102 (1992) 114–127.
[22] B. Gurevich, V.B. Zyrianov, S.L. Lopatnikov, Seismic attenuation in finely layered porous rocks: effects of fluid flow and scattering, Geophysics 62 (1997) 319–324.

[23] M.K. Jain, Numerical Solutions of Differential Equations, Wiley Eastern Ltd., 1984.
[24] D. Kosloff, D. Kessler, A. Queiroz Filho, E. Tessmer, A. Behle, Strahilevitz, Solution of the equation of dynamic elasticity by a Chebyshev spectral method, Geophysics 55 (1990) 734–748.
[25] D. Kosloff, R. Kosloff, Absorbing boundaries for wave propagation problems, J. Comput. Phys. 63 (1986) 363–376.
[26] D. Kosloff, H. Tal-Ezer, A modified Chebyshev pseudospectral method with an $O(N^{-1})$ time step restriction, J. Comput. Phys. 104 (1993) 457–469.
[27] A.R. Levander, Finite-difference forward modeling in seismology, in: D.E. James (Ed.), The Encyclopedia of Solid Earth Geophysics, Van Nostrand Reinhold, New York, 1989, pp. 410–431.
[28] H.M. Mooney, Some numerical solutions for Lamb's problem, Bull. Seism. Soc. Am. 64 (1974) 473–491.
[29] C. Pekeris, The seismic surface pulse, Proc. Natl. Acad. Sci. USA 41 (1955) 469–475.
[30] W.L. Pilant, Elastic waves in the earth, Elsevier, Amsterdam, 1979.
[31] E. Priolo, J.M. Carcione, G. Seriani, Numerical simulation of interface waves by high-order spectral modeling techniques, J. Acous. Soc. Am. 95 (1994) 681–693.
[32] M. Qaisar, Attenuation properties of viscoelastic material, Scattering and attenuation of seismic waves, Part II, in: R.-S. Wu, K. Aki (Eds.), PAGEOPH, vol. 131, Birkhäuser, Basel, 1989, pp. 703–713.
[33] R. Renaut, J. Fröhlich, A pseudospectral Chebychev method for the 2D wave equation with domain stretching and absorbing boundary conditions, J. Comput. Phys. 124 (1996) 324–336.
[34] M. Reshef, D. Kosloff, D. Loewenthal, Elastic wave calculations by the Fourier method, Bull. Seism. Soc. Am. 74 (1984) 875–891.
[35] M. Reshef, D. Kosloff, M. Edwards, C. Hsiung, Three-dimensional elastic modeling by the Fourier method, Geophysics 53 (1988) 1184–1193.
[36] F. Schubert, B. Koehler, Three-dimensional time domain modeling of ultrasonic wave propagation in concrete in explicit consideration of aggregates and porosity, J. Comput. Acous. 9 (2001) 1543–1560.
[37] E. Tessmer, D. Kosloff, 3-D elastic modeling with surface topography by a Chebyshev spectral method, Geophysics 59 (1994) 464–473.
[38] J. Xia, R.D. Miller, C.B. Park, Estimation of near-surface shear-wave velocity by inversion of Rayleigh waves, Geophysics 64 (1999) 691–700.